Applied Geochemistry 27 (2012) 1829–1843

Contents lists available at SciVerse ScienceDirect

Applied Geochemistry

journal homepage: www.elsevier.com/locate/apgeochem

Geochemical and geo-electrical study of mud pools at the Mutnovsky volcano (South Kamchatka, Russia): Behavior of elements, structures of feeding channels and a model of origin

E.P. Bessonova [a], S.B. Bortnikova [b,*], M.P. Gora [a], Yu.A. Manstein [b], A.Ya. Shevko [a], G.L. Panin [b], A.K. Manstein [b]

[a] Sobolev Institute of Geology and Mineralogy, SB of the RAS, 3, Koptuga pr., 630090 Novosibirsk, Russia
[b] Trofimuk Institute of Petroleum Geology and Geophysics, SB of the RAS, 3, Koptuga pr., 630090 Novosibirsk, Russia

ARTICLE INFO

Article history:
Available online 1 March 2012

ABSTRACT

This study presents data on the geochemical composition of boiling mud pools at the Mutnovsky volcano. The physicochemical characteristics of the pools and the concentrations of major, minor and trace elements in pool solutions vary widely. A comparison of the geochemical compositions of host rocks and solutions indicates that leaching from rocks is not the only source of chemicals in thermal solutions. Geophysical studies reveal the inner structure of thermal fields, which reflect the shapes of the underground reservoirs and feed channels. Using geophysical methods (electrical resistivity tomography and frequency domain investigations), it was shown that the vertical structure and complex geochemical zonation of the feed channels leads to a high contrast in the compositions of the mud solutions. These findings answer questions about the origin and composition of surface manifestations. To elucidate the mechanisms of solution formation, an attempt was made to describe the magmatic fluid evolution and the resulting mixing of waters by physical and mathematical models. The model illustrates fluid migration from a magma chamber to the surface. It is shown that the formation of brines corresponding to the mud pool composition is possible during secondary boiling.

1. Introduction

Volcanic fumaroles, crater lakes and acidic Cl–SO_4 springs at volcanic edifices are manifestations of magma degassing. High-temperature fumaroles (>700 °C) usually perform the surface transport of not only common, highly volatile compounds, such as CO_2, SO_2, HCl, HF, but also many metals and non-metals that have high mobilities at high temperatures, including volatile chlorides, fluorides, native metals and more complicated compounds (Symonds et al., 1987, 1994; Bernard and Le Guern, 1992; Taran et al., 2000; Korzhinsky et al., 2002; Zelenski and Bortnikova, 2005). Condensates of high-temperature volcanic gases contain significant concentrations of metals, and sublimates and incrustations at high-temperature fumaroles are similar in composition to high-grade ore bodies that are formed in a magmatic environment (Symonds et al., 1987; Hedenquist, 1995; Taran et al., 1995, 2002). Acid crater lakes are condensers of magmatic gases, but they also develop their chemical compositions through interaction with wall rocks. In many cases of crater lake waters, it is difficult to distinguish the contributions from magma and leached volcanic rocks (Pasternack and Varekamp, 1994; Rowe et al., 1995; Takano et al., 2000; Delmelle and Bernard, 1994; Varekamp et al., 2009). The same is true for acid Cl–SO_4 springs that discharge at the edifices of many volcanoes (Fazlullin, 1999; Shinohara et al., 1993; Taran et al., 1996; Auippa et al., 2001b; Bortnikova et al., 2005).

In many thermal fields with fumarolic activity, one can find other thermal manifestations, including hot springs, boiling water pools and mud pools. Mud pools usually lack drainage systems and discharge only vapor into the atmosphere. These pools in volcanic craters differ from those in the thermal fields of meteoric hydrothermal systems due to their low or very low pH and high mineralization of water. Their water is often similar in composition to volcanic gas condensates, acid Cl–SO_4 waters of volcanic springs and waters from acid crater lakes, indicating a strong magmatic contribution to the mud pool water.

At least 10 mud pools lacking drainage can be found on the crater floor of the Mutnovsky volcano, an active volcano of South Kamchatka that is located 75 km south of the city of Petropavlovsk–Kamchatsky. Mutnovsky is characterized by strong fumarolic activity, with an SO_2 flux of approximately 200 t/d

* Corresponding author.
E-mail address: bortnikovasb@ipgg.nsc.ru (S.B. Bortnikova).

0883-2927/$ - see front matter © 2012 Elsevier Ltd. All rights reserved.
doi:10.1016/j.apgeochem.2012.02.018

(Taran et al., 1992; Zelenski and Taran, 2011). The study presents information on the chemical composition of a set of mud pools of Mutnovsky that includes major and trace element chemistry and estimations of their relative contributions to mud pools from different sources. Results are also presented of a high-resolution resistivity survey of the crater floor that can be interpreted in terms of the shallow structure of the volcano-hydrothermal system and reveals the existence of a shallow aquifer and a system of conduits feeding mud pools and other thermal manifestations of the volcano crater.

2. Mutnovsky volcano and its thermal manifestations

The Mutnovsky volcano (main summit at 52°21′N, 158°16′E; absolute altitude of 2323 m) is located 75 km south of the town of Petropavlovsk–Kamchatsky (Fig. 1). The volcano is currently one of the most active volcanoes of the Kamchatka volcanic belt. Two merged craters are located to the NW and west of the summit. Among several known historical eruptions, two have been described in detail: 1960–1961 (Vakin et al., 1966) and March 17, 2000 (Zelenski, 2003). Between eruptions, the volcano is characterized by intense fumarole activity. Three fumarole fields are located in the eastern crater: (1) upper (Verkhneye) field, with vent temperatures of up to 280 °C; (2) bottom (Donnoe) field, consisting of two relatively separate areas with temperatures up to 260 °C; and (3) active funnel, where the temperatures of powerful gas jets reached up to 620 °C in 2006 (Zelenski and Taran, 2011). The compositions of the gases and hydrothermal solutions of this volcano have been studied since 1961 (Vakin et al., 1966; Serafimova, 1979; Trukhin et al., 1986; Taran et al., 1991, 1992; Zelenski et al., 2002; Zelenski and Bortnikova, 2005; Zelenski and Taran, 2011).

The Donnoe fumarolic field of the volcano (northeastern crater) is the bottom of a dried lake. At the present time, the Donnoe fumarolic field, which has hydrothermally altered rocks, has an almost flat topography. There are numerous strong boiling and bubbling springs with temperatures of 80–97 °C that are located in this fumarolic field. Thin steaming jets and vapor emerge from the hottest sites in the field (hereafter referred to as hot sites). The ground temperatures reach 67 °C. Wet deposits in the hot sites are apparently a sand-clay type mixture of profoundly altered rocks and are saturated by saline solutions. The surfaces of the hot sites are covered by newly formed mineral efflorescences that are largely composed of sulfates. Three fumaroles with sulfur domes, a large black mud pool, and a number of small thermal springs and mud pools are generally constantly active. Their temperatures, colors (and transparency), and consistency (water/mud ratio) vary widely, from small transparent outcrops of boiling water to black mud pools (with the proportion of suspended matter as high as 10%). Mud pools with boiling mixtures of yellowish, whitish or greenish color occur there. The distances between individual mud pools do not exceed 2–3 m. A glacier and snowfields are located on the slope of the crater, supplying water to a stream that flows into the field, mixing with some of the pools.

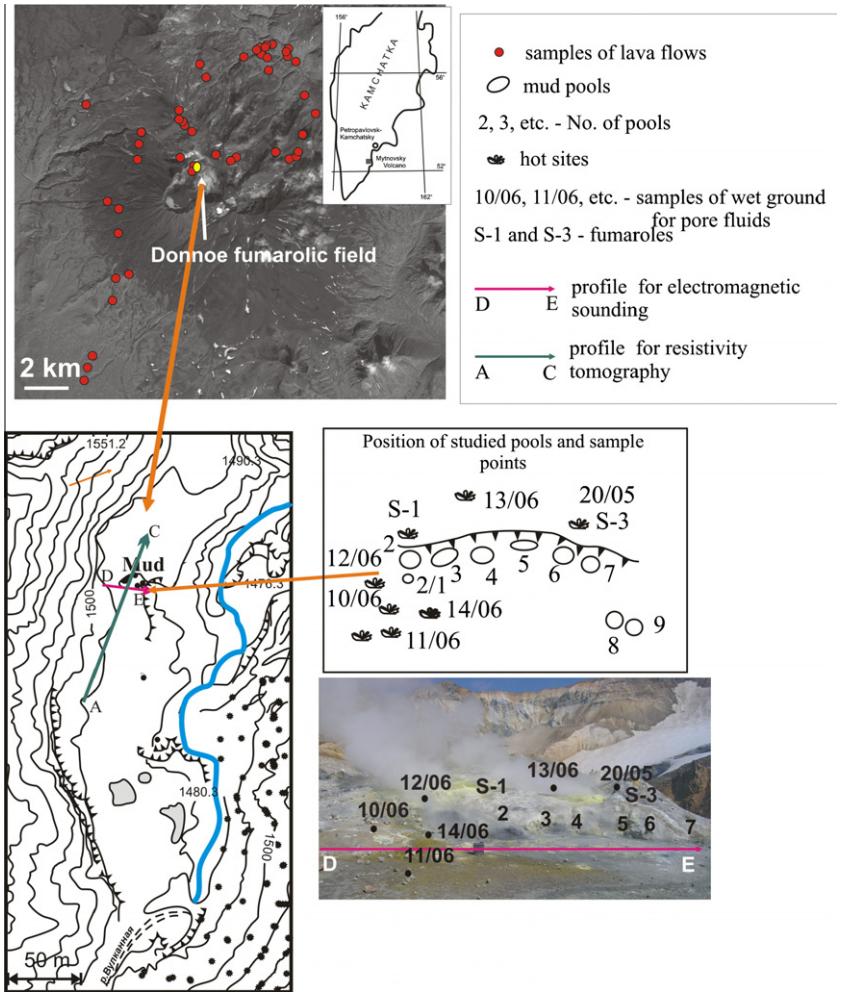

Fig. 1. The Mutnovsky volcano, with sampling points in the Donnoe fumarolic field and geo-electrical profile trends.

The detection of anomalously high concentrations of elements in pool liquids revealed a problem regarding their origins and led to monitoring this abnormality for several years. The authors studied the Donnoe field as an integral system in which each component interacts with other components. In addition to the pool fluids, the compositions of pore liquids from the hot sites and fumarole domes in the vicinity of the pools were analyzed. It is clear that these liquids have common sources of gas and heat. Condensates and pore liquids were collected from the inner parts of the fumarole domes. In this study, the results of the investigations of major, minor and trace element behavior in different surface manifestations of magmatic fluid: the gaseous phase as condensates of fumaroles and (residual) liquids from boiling pools, are presented. Geophysical investigations revealed the subsurface structure of the fumarolic field and enabled tracing the subsurface hydrogeochemical zonation. Physicochemical modeling provides an understanding of the processes and mechanisms of element extraction, transport, and partitioning during fluid ascent from the magma chamber to the surface.

3. Approach and testing methodology

3.1. Field sampling and geo-electrical sounding

Various sampling campaigns were carried out over a period of 6 years (2005–2010). Ten sampling points were monitored, including liquids from different mud pools of the Donnoe fumarole field, which show large variations in geochemical parameters. The locations and salient features of the mud pools are shown in the sketch of the sampling points (Fig. 1).

Water and mud from the pools were collected in a Teflon sampler and packed into plastic boxes, avoiding any contact with metals. Values of pH, Eh, temperature and electrical conductivity were measured at the sampling sites after the suspended solids settled out of the liquids. Values of pH and Eh were measured with a HANNA HI 9025C portable pH meter, electrical conductivity was measured with a Cond 315i/SET device (WTW, Germany), and temperature was measured with a LT-300 thermometer (Termex Ltd., Russia). The concentration of Fe(II) was measured with a HACH DR/890 portable colorimeter. The levels of NO_3, NO_2, NH_4, Cl, and F were measured by the Econics-Expert ionometer *in situ* and later confirmed for selected samples under laboratory conditions. Samples for major and trace element analysis were filtered through 0.45-μm membrane filters. Acidification with HNO_3 was not required, as all samples were either acidic or hyper-acidic.

Another group of samples included the following: (i) wet deposits of hydrothermally altered rocks from hot sites at the Donnoe field; (ii) condensates from sulfur fumaroles; and (iii) native sulfur from the interiors of fumarole domes. These native sulfur samples were also collected to squeeze pore water from them under laboratory conditions. Samples of wet ground material were collected from small pits that were 10–15 cm in depth. Condensates were sampled using a glass condenser cooled with ice water.

To appraise the geochemical behaviors of elements during volcanic rock weathering processes, samples of unaltered rocks were collected from the earliest to the latest phases of volcanic activity. Unaltered rocks that are representative of all Mutnovsky lava flows (as identified on the geological map and cross section, Selyangin, 1993) were sampled from different parts of the volcano (Fig. 1).

Geophysical studies were conducted in 2007 and 2009 using the electromagnetic frequency induction sounding (NEMFIS) technique developed by Trofimuk Institute of Petroleum Geology and Geophysics, Siberian Branch of Russian Academy of Sciences IPGG SB RAS (Russia). The prerequisite for the application of electromagnetic sounding is the high levels of total dissolved solids (TDSs) of liquids (which was the case for thermal waters in the Mutnovsky volcanic area) and, therefore, high electric conductivity of the subsurface media. Under these conditions, the problem of identifying thermal water channels in the mountainous region was reduced to the detection of the conductive electrolyte in the parent medium with relatively low specific electric resistivity (Manstein et al., 1983, 2006). The combination of electromagnetic sounding and geochemical mapping of active volcanoes has been used extensively to assess the presence and spatial distribution of groundwater reservoirs and hydrothermal systems (Zlotnicki et al., 2009; Finizola et al., 2010; Fournier et al., 2011).

The area of study in the Donnoe field was divided into measurement points on a grid of 1×1 m (Fig. 1, profiles D–E). The soundings were performed at 14 frequencies, ranging from 2.5 kHz to 250 kHz. The data obtained were processed by ISystem software, which is part of the NEMFIS tool. The length of each profile was 29 m. The 2D distributions of apparent specific resistivity (ρ) were plotted on the cross sections.

To achieve deeper penetration of the geophysical survey, resistivity tomography was applied using the SibER resistivity meter (developed by IPGG SB RAS). The observation line was across the mud pool axis and the profile of electromagnetic sounding (Fig. 1, profiles A–C). Geo-electrical resistivity tomography measurements were obtained using a set of 48 steel electrodes that were spaced every 5 m. The total length of the profile was 235 m. The electrode contact resistance was provided by saline pore water. The Wenner-alpha array was used because of its good signal-to-noise ratio. The geo-electrical cross sections at a depth of 40 m were performed using a 2D inversion by Geotomo software RES2DINV software.

3.2. Laboratory analyses

In the laboratory, pore liquids were squeezed out of the samples of hydrothermally altered rocks and from the samples from fumarole domes under 100 bars pressure. Samples were split, and half of each sample was filtered through 0.45-μm membrane filters for 1 day.

Major anion (Cl, F, SO_4, and NO_3) and NH_4 analyses were carried out on unfiltered samples using ion chromatography. Major cation (Al, Fe, Ca, Mg, K, Na, and Si) and trace element (including P) analyses were carried out using ICP-AES (IRIS Advantage) at the Analytical Center at IGM SB RAS. The error in the ionic balance was less than 15%. To analyze a concentrated substance, dry salts were obtained by evaporating several samples (collected in 2007 and 2009) at 105 °C.

The bulk rock composition was determined using an X-ray fluorescence (XRF) method for 53 samples at the Analytical Center at IGM SB RAS. The trace element concentrations in rocks and dry salts were determined in pressed pellets of 30 mg using XRF with synchrotron radiation (Baryshev et al., 1986) at station VEPP-3 at the Institute of Nuclear Physics SB RAS, Novosibirsk, Russia. Measurements were made at an activation energy of 30 keV using internal standards. Issue spectra processing was performed using the AXIL program. The definition error was 15–20%.

3.3. Numerical modeling

The software package which was developed for this study combines the SP Selector (Karpov et al., 2002) and SP Fluid (Sharapov et al., 2008) codes. It was developed to simulate a model using all available complex data from the fields of thermophysics, hydrodynamics and physical chemistry. The SP software is a numerical, quasi-2D model based on non-isothermal physicochemical dynamics of fluid–rock interactions accompanied by the phase changes that occur during magmatic fluid flow. The numerical model was

built by combining two main features: the Stefan approach, for the description of the appearance and disappearance of the phase interfaces in fluid flow within porous fractured medium, and a descriptive methodology of equilibrium physicochemical dynamics (within the scope of a flow reactor approximation) realized in the SP Selector code. First, thermophysical and hydrodynamic parameters were calculated in all reactors for each time point. These parameters were used to determine the physicochemical equilibrium in the direction of the fluid "wave" propagation through a multiple-reactor column. This approach allowed, for the first time, taking the real time measurements (counted from the generation of a magma chamber) instead of "conditional time" measurements, which have been used in similar computer codes.

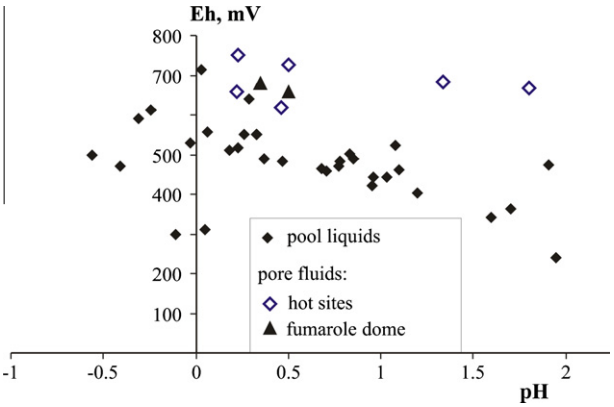

Fig. 2. Eh–pH diagram for mud pool discharges and pore fluids.

4. Results and discussion

4.1. Solution geochemistry

The temperatures in the mud pools range from 60 °C to 96 °C but remain constant in a particular pool from year to year. Temperature is the most stable parameter for pools, implying constant feeding of hot fluids to the surface. All pool discharges correspond to acid or hyper-acid waters (pH values range from −0.56 to 1.95), whereas the Eh values (240–715 mV) suggest oxidizing conditions (Table 1, Fig. 2). Conductivity values range from 10 mS/cm to more than 600 mS/cm, indicating high but varying levels of TDS in the solutions.

The variation in TDS over a wide range, from 4900 mg L^{-1} to more than 80,000 mg L^{-1}, is negatively correlated with acidity ($r = -0.464$). The major anions of all sampled pool discharges were SO_4^{2-} and Cl^-; very high Cl^- concentrations (up to 79 g/L) were the main feature of the Donnoe pools. Earlier studies (Giggenbach, 1996; Shinohara et al., 2008) have shown that the Cl-rich composition of volcanic gases suggests magma degassing. High concentrations of Cl^- in pool discharges can be attributed to an input of magmatic gases from a shallow magma chamber.

There is a strong positive correlation between TDS and Cl^- and an absence of any correlation between TDS and SO_4^{2-} in the same

Table 1
Physico-chemical parameters and concentrations of major ions in mud pool discharges at Donnoe field, in mg L^{-1}.

Year and sample no.	*X*, mS/cm	*T*, °C	pH	Eh	Cl^-	F^-	SO_4^{2-}	PO_4^{3-}	NO_3^-	Na^+	K^+	Ca^{2+}	Mg^{2+}	NH_4^+	Fe^{3+}	Fe^{2+}	SiO_2	Al
2005																		
2	na	87.4	0.03	715	56,000	1.9	2300	37	nd	133	200	110	29	nd	140	190	100	720
2006																		
2	na	87.3	−0.24	612	34,000	2.03	1600	33	bdl	190	190	270	110	2.5	150	180	190	1670
2/1	na	72.5	−0.56	500	27,000	3.7	590	27	bdl	160	240	230	100	4.3	160	150	87	800
3	na	87.7	−0.31	590	31,000	5.2	3300	40	48	150	200	150	53	4.1	20	150	220	1860
4	na	83	0.18	510	13,000	30.2	2700	15	69	67	120	53	17	13	14	50	270	1100
5	na	84	−0.03	530	31,500	115	8500	120	3.0	500	740	170	46	33	30	160	240	2700
6	na	62.5	1.95	240	2500	0.009	650	0.68	bdl	5.5	7.3	40	1.4	0.25	3.1	4.5	7.9	170
7	na	75.5	0.33	550	18,400	25	2700	45	91	160	41	700	160	1.9	220	170	400	2300
8	na	76.4	0.05	310	3200	0.12	700	21	7.1	100	130	62	19	7.3	16	40	250	750
9	na	75.8	−0.11	300	15,000	0.25	2200	65	bdl	270	380	120	39	30	10	130	320	1870
9/1	na	69.5	0.29	640	2700	25	630	19	4.0	97	120	70	24	7.7	14	50	230	880
2007																		
2	478	88	−0.41	472	74,000	2.1	1000	5.6	56	39	60	98	24	3.5	40	110	100	196
2/1	340	88	0.11	445	44,000	3.4	1200	7.4	32	42	25	99	38	2.8	50	110	124	248
3	523	88	0.06	556	37,000	0.2	1750	16	120	92	64	190	57	2.4	37	130	86	500
4	628	86	0.26	552	17,000	67	5300	27	90	100	130	140	45	6.7	160	280	100	700
5	186	86	0.85	488	8400	5.8	1200	65	46	200	670	77	24	17	50	150	200	1510
6	160	60	1.91	474	7600	7.6	1100	bdl	12	2	0.8	54	2.1	0.1	0.9	3.2	3.8	120
2009																		
2	140	94	1.1	462	22,000	bdl	6400	15	290	87	52	210	53	3.2	170	200	330	380
3	210	93	0.96	442	40,000	bdl	630	11	510	70	39	180	46	1.8	50	170	270	315
4	180	88.7	0.95	422	38,000	bdl	350	10	960	65	36	130	43	0.82	69	76	320	311
5	310	92.9	0.78	482	64,000	0.001	640	18	840	140	150	160	50	1.06	150	46	270	690
6	120	77.8	1.03	442	26,000	bdl	640	17	230	120	156	130	36	1.9	180	110	360	620
8	52	86.8	1.2	402	5900	bdl	230	11	79	62	54	120	41	1.4	290	180	440	430
9	10	94	1.6	342	898	bdl	500	4	19	13.6	17	440	13	0.12	160	80	110	110
2010																		
2	315	92	0.23	318	43,700	na	2460	5.7	na	54	31.8	110	40.1	na	75	320	131	300
2/1	124	89	0.47	282	11,500	na	1700	11	na	86	62.2	157	61.9	na	50	110	332	610
3	230	92.5	0.37	287	9437	na	1300	5.9	na	54	35.9	88	35.0	na	20	100	210	340
4	149	85.7	0.71	255	12,323	na	1025	6.9	na	59	33.9	102	37.6	na	4	110	293	340
5	230	87	0.68	262	20,499	na	1430	7.7	na	112	114.4	139	38.7	na	26	85	297	480
6	152	78	0.77	269	10,308	na	1310	6.4	na	84	87.2	108	30.7	na	32	78	320	390
7	24.1	83	1.08	322	1244	na	2000	1.9	na	21.7	11.7	118	18.6	na	14	33	440	140

Hereinafter the sample no. corresponds to the No. of pool (see scheme of sampling in Fig. 1); na: not analyzed; bdl: below detection limit.

pools (Fig. 3). The Cl^- concentration exhibited changes in magnitude of 1.5–3.0 – fold over 5 years of observation, with corresponding changes in the TDS values. The variations in TDS and Cl^- concentrations demonstrate a dependence of pool discharge compositions on meteorological conditions, i.e., the degree of magmatic fluid dilution by meteoric waters that are supplied by thawing snowfields. The Cl^- concentration increases with decreasing pH, while the SO_4^{2-} concentration varies randomly. The levels of the other halogens found in the pool discharges were *F*, up to 115 mg L^{-1}; I, up to 42 mg L^{-1}; and Br, up to 4.0 mg L^{-1}. As pointed out by Villemant et al. (2008), the degassing paths of H_2O and halogens in andesitic magmas are similar. Fluorine is not extracted in the gas phase. However, other halogens and H_2O are strongly depleted during magma degassing, but Cl, Br and I are not fractionated with respect to each other. Phosphate and NO_3^- concentrations vary and reach up to 120 and 960 mg L^{-1}, respectively. The anion composition of the pool liquids indicates that the discharges are mixtures of different acids: they are mainly HCl and H_2SO_4, with significant amounts of HNO_3, HF, H_3PO_4 and HI.

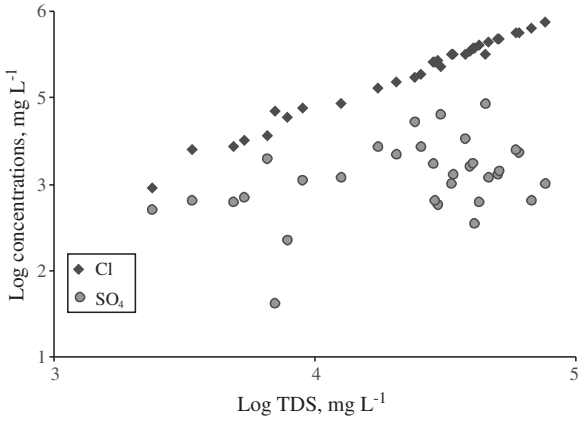

Fig. 3. Log-log plots for the concentrations of chloride and sulfate versus TDS.

The second unique feature of the studied pools is the high proportion of Al in all pools: 66–90 equivalent% of cations. The maximum concentration of Al is 2700 mg L^{-1}, which is comparable to the Al concentration of hyper-acidic brines at the Kawa Ijen volcano (Hinsberg et al., 2010). Alkali (K and Na) and alkaline earth (Ca and Mg) metals, which are usually the major cations in natural waters, account for a minor proportion of cations in these pool discharges. In some pools, the second major cation is Na, and in two pools, the second major cation is Ca. Iron is an important constituent in the discharges, with a level of up to 10 equivalent%. As a rule, Fe(II) dominates over Fe(III), despite the oxidizing conditions of the solutions.

The third unique feature of the mud pool solutions is the high concentrations of many trace elements, especially Cr, Ni, Co, Ti and V (Table 2). The maximum Cr level (60 mg L^{-1}) and very high Ni and Co concentrations (33 and 0.48 mg L^{-1}, respectively) are found in pool no. 2; this pool has the highest recorded concentrations of these elements in acidic volcanic waters. The concentrations of these elements vary from several fold to three orders of

Table 2
Trace element data for solutions of mud pools, mg L^{-1}.

Year and sample no.	B	Mn	Ba	Li	Sr	Rb	Zn	Cu	Ti	V	Co	Cr	Ni	As	Sb	Mo
2005																
2	52	5.5	0.24	0.037	5.6	bdl	0.45	0.62	4.2	2.4	0.48	60	33	0.39	bdl	0.39
2006																
2	160	5.9	1.8	0.07	5.5	0.015	0.69	0.06	15	2.6	0.08	0.39	0.11	0.36	0.65	bdl
2/1	130	5.5	1.5	0.06	4.3	0.012	0.67	0.02	10	2.2	0.08	4.6	1.9	0.06	bdl	0.02
3	33	2.8	1.9	0.06	6.5	0.015	0.43	0.06	7.9	2.3	0.03	0.38	0.12	0.12	bdl	bdl
4	9.1	1.1	1.0	0.05	2.1	0.01	0.18	0.01	0.78	0.92	0.02	2.3	0.93	0.23	bdl	bdl
5	32	3.0	0.63	0.16	20	0.52	0.39	0.050	3.2	4.5	0.05	5.0	1.8	0.61	bdl	0.03
6	0.53	0.07	0.05	0.001	0.17	bdl	0.09	0.02	0.02	0.040	0.002	0.14	0.080	bdl	bdl	bdl
7	30	5.3	0.36	0.06	12	0.0062	1.3	0.25	1.2	5.4	0.05	4.4	1.6	0.50	bdl	0.021
8	9.0	1.0	0.38	0.03	2.7	bdl	0.4	0.04	0.88	1.0	0.010	0.92	0.38	bdl	bdl	bdl
9	17	2.0	0.29	0.09	11	0.27	0.58	0.09	5.1	2.8	0.030	0.57	0.07	bdl	bdl	bdl
9/1	8.2	1.1	0.36	0.04	2.2	bdl	0.36	0.03	0.74	0.99	0.010	0.25	0.06	bdl	bdl	bdl
2007																
2	120	3.0	2.13	0.07	2.8	0.08	0.31	0.28	5.9	0.78	0.07	6.4	3.2	0.11	0.067	0.05
2/1	130	2.3	2.7	0.01	1.9	bdl	0.24	0.06	5.5	0.97		3.9	1.9	bdl	bdl	bdl
3	49	3.3	2	0.02	3.1	0.05	0.37	0.26	7.1	1.4	0.11	4.4	1.8	bdl	0.11	0.02
4	33	5.3	0.81	0.03	6.0	0.14	0.4	0.25	6.3	1.8	0.16	20	7.9	bdl	0.03	0.22
5	6.5	3.2	0.19	0.07	14	0.46	0.7	0.28	0.98	2.9	0.1	16	13	bdl	0.010	0.12
6	0.14	0.03	0.02	bdl	0.1	bdl	0.06	0.01	bdl	bdl	bdl	bdl	0.03	bdl	bdl	bdl
2009																
2	50	2.4	0.47	0.10	2.7	0.18	1.0	0.48	0.58	1.2	bdl	6.6	3.0	bdl	0.0016	0.34
3	37	2.1	0.79	0.03	2.1	0.03	0.26	0.026	1.0	0.93	bdl	5.1	2.7	bdl	0.00038	0.59
4	13	1.9	0.44	0.032	1.7	0.03	0.29	0.19	1.3	0.75	0.038	3.3	1.6	bdl	0.0006	0.51
5	18	3.0	0.37	0.13	4.4	0.19	0.55	0.22	2.5	1.3	0.14	13	6.7	bdl	0.021	0.51
6	7.7	1.5	0.21	0.11	3.7	0.13	0.60	0.34	0.72	1.0	0.026	2.1	0.96	bdl	bdl	0.38
8	4.7	2.6	0.53	0.045	2.0	0.09	1.4	0.58	0.15	0.98	0.12	14	7.5	bdl	0.0016	0.085
9	1.4	0.49	0.13	0.025	1.3	0.02	0.20	0.05	0.14	0.18	0.033	0.11	0.12	bdl	bdl	1.0
2010																
2	25	8.10	0.97	0.025	1.6	bdl	0.491	0.88	4.18	0.99	0.36	60	19	0.90	bdl	0.12
2/1	43	2.94	0.66	0.047	2.4	bdl	0.41	0.049	1.25	1.40	0.031	2.5	1.1	0.83	bdl	bdl
3	14	2.27	1.19	0.035	1.2	bdl	6.9	0.041	1.28	0.73	0.08	7.5	4.2	0.41	bdl	bdl
4	15	1.98	1.00	0.031	1.3	bdl	1.5	0.11	0.99	0.75	0.037	3.8	2.2	0.39	bdl	0.05
5	16	2.01	0.42	0.046	3.4	bdl	1.7	0.005	1.79	0.82	0.016	0.21	0.08	bdl	bdl	bdl
6	11	2.07	0.42	0.037	2.4	bdl	0.55	0.022	1.04	0.69	0.056	5.5	2.4	0.26	bdl	bdl
7	2.6	0.64	0.083	0.025	0.41	bdl	0.34	0.007	0.045	0.37	0.004	0.06	0.011	0.26	0.1	bdl

magnitude in different pools. The layout of the pools is intriguing: they are aligned for 20 m, with less than a few meters between pools. Pool compositions vary significantly over the years. Element concentrations changed from 2–5 times to 1 order of magnitude for certain pools during the study period. Time series trends are plotted in Fig. 4. The long-term variations in element concentrations can be explained by unsteady levels of saturation of meteoritic water with deep magmatic gases. This input from surface waters is governed by current meteorological conditions (volume of precipitation, temperature, presence or absence of the snowfields). The TDS values and conductivity of the discharges are indirect indicators of the degree of dilution of magmatic fluid with meteoric waters. However, a strong correlation between the concentrations of Cr, Ni, Co, Ti, and V and TDS was not observed, both in terms of annual variation and from pool to pool. Another reason for the wide range in element concentrations may be the complicated routes of the ascent of thermal water through the subsurface space and the subsequent differences in the fluid composition at geochemical barriers. This assumption is supported by a relatively constant average concentrations of the metals sampled in different pools (Fig. 4). This stability of metal concentrations implies relatively constant metal concentrations in the underground reservoir that feeds the surface manifestations. However, during the ascent of thermal waters, different quantities of metals enter different channels. This phenomenon is manifested in a varying composition of surface pool waters.

The composition of the pore fluids from hot sites (Table 3) is significantly more homogenous than the compositions of the mud pool discharges (Table 2). The pore fluids are highly saline brines, with TDS values of 16–95 g L^{-1}. The ratio of Cl/SO_4 for the pore fluids is lower than the ratio for the pool discharges, due to a lower Cl concentration and to a higher SO_4 concentration. The high PO_4 concentration is noteworthy. The concentrations and ratios of the major cations (K, Na, Ca, Mg, Fe, and Al) are also different from those in the pool liquids. The pore space is saturated with brines of a unique composition. The concentrations of Cr and Ni in the pore liquids are lower than those in the pool fluids, but the levels of Co, Ti and V are extremely high.

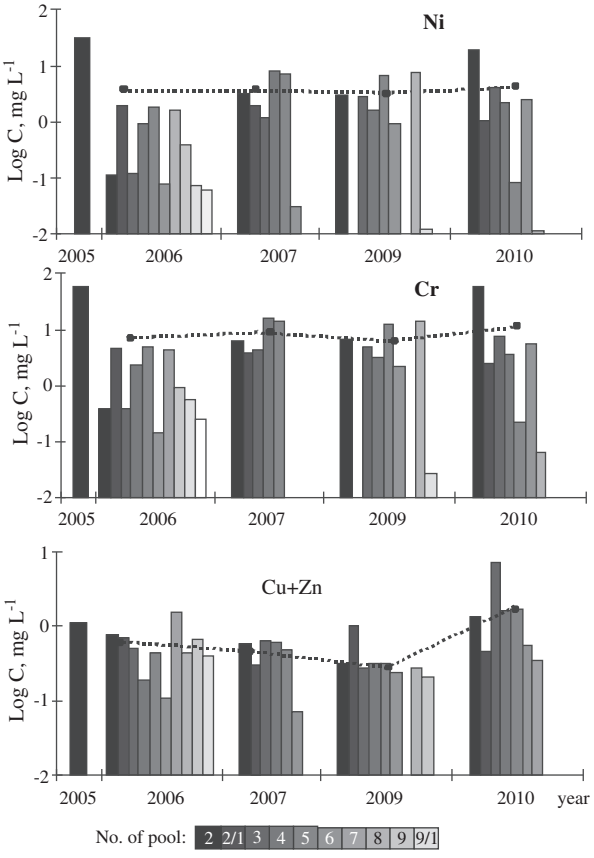

Fig. 4. Concentrations of metals in mud pools from 2005 to 2010. The dotted lines indicate average concentrations. The bars on this diagram correspond to the number of pools sampled. In dry years, some pools cease to exist.

The compositions of the pore solutions from the sulfur fumaroles are distinct from pool liquids (Table 3). The major anion and cation are Cl^- and NH_4^+, respectively. The trace element concentrations are lower than those in pore fluids from hot sites, except for those of Ba, Sb and As. Condensates from these sulfur fumaroles are low-saline acid fluids with low concentrations of major and trace elements.

Pore solutions that are collected at vapor emission areas originated from uprising fluids (brines were concentrated due to intensive evaporation). This area is considered to be a shallow geothermal barrier where the phase separation of fluid of liquid and gas takes place. Meanwhile, the vertical fractures piercing the barrier are the zones of pressure drawdown. Finally, some portions of the uprising fluids discharge into the boiling mud pools. As the fluid travels through vertical channels to the surface, it is enriched by pore solutions captured from the surrounding rock. These fluid dynamics alter the composition of the pore solutions: the final compositions of the samples are the result of evaporation at the surface and lateral filtration of fluid from the porous walls. The same principle describes a fumarole, where the fluid is separated into a volatile gas mixture, and the liquid is captured in the pores.

The trace elements compositions show distinctive characteristics that can help to ascertain the origin of mud pools by way of extremely high TDS and trace element concentrations in the pools and the variation in element concentrations from pool to pool. Extremely high TDS and concentrations of trace elements in the pools indicate an interaction between hydrothermal solutions and volcanic rocks. To explain the variability in element concentrations, the subsurface structure was examined using geophysical methods. The two methods were applied to depths of 7 and 40 m.

4.2. Rock geochemistry

Rocks of the Mutnovsky volcano were studied in detail. Samples of the entire suite of rocks present was collected from the edifice and basement of the volcano. The bulk rock composition is reported in Table 4. The main feature of the Mutnovsky lava flows is their large range in bulk composition, which extends from basalts to rhyolites (Selyangin, 1993). Attention was focused on basalt and basaltic andesite because these are the most common rocks in the volcano. The main feature of the basalt and basaltic andesite compositions is the wide variety of major and trace element concentrations. The flow of olivine basalts was traced on the volcano basement. These olivine basalts differ from the basalts of the Mutnovsky edifice due to their elevated MgO concentration, which reaches 8.1%.

The trace element concentrations also varied widely in the studied rocks (Table 4). The association between the elements of interest, Ti, V, Cr, Ni, and Co, is characteristic of basalts. The concentrations of these elements in acid-effusive rocks were low compared to the concentrations found in basalts. Titanium and V showed negative correlations with SiO_2 ($r = -0.59$ and -0.69, respectively) but a positive correlation with Fe ($r = 0.79$ and 0.76, respectively) due to their tendency to concentrate in titanomagnetite. In contrast to Ti and V levels, the Cr concentration in the rocks depended on the MgO concentration. The highest concentrations of Ni and Cr were found in MgO-rich olivine basalts that were

Table 3
The composition of pore fluids and condensates, mg L^{-1}.

	Pore fluids hot sites						Pore fluids from fumarole domes		Condensates	
	20/05	10/06	11/06	12/06	13/06	14/06	S-1	S-3	K-1	K-2*
T°							110	137		
pH	0.23	0.5	0.46	1.8	0.22	1.34	0.5	0.35	0.8	na
Eh	750	726	619	669	659	682	660	680	190	na
Cl^-	6800	7300	1900	8400	15,000	6000	21,000	24,400	6900	2400
SO_4^{2-}	8700	11,000	14,000	9200	12,000	9000	660	2560	42	57
PO_4^{2-}	920	6600	1240	4300	4200	11	15	23	nd	bdl
Na^+	1450	5500	5400	7400	6400	93	110	71	3.3	0.5
K^+	120	350	400	410	380	110	80	30	1.1	1
Ca^{2+}	53	96	70	70	84	180	220	370	19	200
Mg^{2+}	1850	10,300	5300	7300	8100	71.3	110	84	3.2	2.5
NH_4^+	na	110	67	20	110	150	4020	10,500	bdl	na
Fe_{total}	1120	52,900	9500	23,300	16,500	820	310	400	3.3	0.35
SiO_2	8.4	20	5.9	8.6	13	50	36	59	5	12
Al	6020	14,800	9900	7300	14,300	400	490	680	2.8	0.66
Mn	30	400	91	140	230	3.7	5.3	4.3	0.17	0.027
Ba	bdl	0.21	0.13	0.13	0.06	0.47	6.1	3.9	0.098	2.4
Li	2.5	13	8.4	14	14	0.03	0.04	0.08	bdl	0.0011
Sr	3.7	4.6	3.5	5.2	7.2	1.7	1.8	2.8	0.10	0.16
Rb	bdl	0.57	0.26	0.48	0.39	bdl	bdl	bdl	bdl	0.00076
As	21.3	82	67	12	17	0.95	26	150	bdl	0.16
Sb	bdl	0.25	0.01	0.089	0.1	bdl	5.03	7.2	bdl	bdl
Bi	bdl	0.4	0.34	0.21	0.14	bdl	0.033	0.092	bdl	0.00024
Se	bdl	0.05	0.032	0.065	0.092	bdl	0.07	0.084	bdl	bdl
Zn	38	110	33	36	73	2.8	2.4	1.6	1.10	6.1
Cu	5.4	120	14	13	15	6.1	0.85	2.3	0.006	0.015
Pb	bdl	bdl	bdl	bdl	bdl	0.5	0.3	0.19	0.052	0.1
Ti	114	180	270	360	100	5.1	5.7	7.2	0.008	bdl
V	140	430	280	370	350	1.1	1.4	1.9	0.010	bdl
Co	3.4	5.2	1.5	2.5	1.4	1.1	0.12	0.2	0.006	0.0011
Cr	11.2	18	8.5	11	18	0.33	0.19	0.36	0.04	bdl
Ni	3.5	7.1	1.4	3.5	2.7	0.47	0.11	0.19	0.29	0.003
Be	0	0.99	0.7	0.81	0.89	bdl	0.003	0.0035	bdl	0.0005
B	90	450	110	89	340	29	330	290	12.3	15
Zr	0.26	2.6	31	6.1	1.5	0.33	0.11	0.37	bdl	0.00081

* Data from M.E. Zelenski, unpublished.

sampled from the basement of the volcano edifice (Table 4, samples MT-29, MT-60 and MT-44). The maximum concentrations of Ni and Cr were one order of magnitude higher than the average concentrations of these elements in the Mutnovsky basalts. The MgO-rich olivine basalts are a probable source of certain elements in magmatic fluids and, consequently, in thermal surface manifestations. The results of microprobe tests on minerals showed that the main host mineral for Ni (in basalts) is olivine. The Ni concentration in olivine from the Mg-basalt (MT-29) reaches 0.3%, unlike other basic rocks of Mutnovsky, in which the Ni concentration in olivine is a maximum of 0.15%. The source of Cr is chromites, which form mineral inclusions in olivine. Titanium and V are released into solution from titanomagnetite.

4.3. Relative mobility of elements

Element mobility was estimated for different rocks of the Mutnovsky lava flows. Log–log plots for dissolved major, minor, and trace elements in liquids from all pools vs. rock compositions are shown in Fig. 5. This approach has been applied to thermal aquifers of the El Chichon volcano (Auippa et al., 2001a; Taran et al., 2008; Hinsberg et al., 2010). The slanting lines on the diagrams correspond to 1, 10, 100 and 1000 g of complete rock dissolution. The most mobile elements in the magmatic fluid/volcanic rock interaction are halogens (Cl, I and Br), B and S. Close in mobility are anion-forming elements (As and Sb) and some metals (Mo and Ag). This finding suggests that these elements have an external source: magmatic gases feed halogens, S, and anion-forming elements into hydrothermal solutions. Many rock-forming elements (Mg, Ca, Si, Ti and Mn) can reach high concentrations in solutions by large-scale hydrothermal weathering, during which time approximately 10 g of basalt will be dissolved in 1 L of solution (e.g., in pool no. 2). However, the concentrations of Cr, Ni, Zn and Ba in the solution are excessive even if 10 g of basalt/L have been dissolved. As suggested by previous studies of volcanic acid underground water (Delmelle and Bernard, 1994; Villemant et al., 2008), the anion composition and pH are determined by volcanic gas inputs. Cations are primarily derived from rock alteration, either directly or through an intermediate hydrothermal system. However, simple whole rock dissolution does not provide the full contribution of elements to the mud pools in the Donnoe field. The concentrations recorded in the pool solutions cannot be reached by leaching from basalt alone (even from basalt MT-29, which has the highest concentrations of trace elements). An additional source of elements or a special mechanism of solution concentration is needed.

The "enrichment factors" approach has been applied to volcanic gases (Symonds et al., 1987), volcanic waters (Taran et al., 1995, 2008) and the crater lake Keli Mutu in Indonesia (Pasternack and Varekamp, 1994). The enrichment factor is usually defined as follows:

$$F_i = (E_i/E_{ref})f/(E_i/E_{ref})_r,$$

where E_i is the concentration of element i, E_{ref} is the concentration of a reference element, and the subscripts f and r stand for fluid and rock, respectively. Magnesium is commonly used as a reference element because of its low mobility at high temperatures. The Mg concentrations in the hot spring fluids are a direct reflection of water–rock interactions in the hydrothermal system, as no

Table 4
Concentrations of rock-forming oxides (in wt.%) and trace elements (in ppm) in rocks of the Mutnovsky volcano.

Component	Olivine basalts and andesite-basalts on the volcano basement			Basalts			Andesite-basalts		Andesites		Rhyolite-dacite
	MT-29	MT-60	MT-44	MT-65	MT-2	MT-24	MT-41	MT-7	MT-4	MT-22	MT-15
SiO_2	51.05	52.15	53.61	50.89	50.21	50.12	52.10	54.46	58.84	61.58	69.84
TiO_2	0.84	0.91	0.94	1.02	1.00	1.15	1.32	1.02	0.82	1.02	0.57
Al_2O_3	16.73	16.38	16.14	19.02	19.97	17.68	16.77	17.28	16.97	16.52	14.21
Fe_2O_3	9.73	9.99	9.88	10.13	10.32	11.34	11.76	9.68	7.52	7.93	4.56
MnO	0.15	0.17	0.17	0.17	0.18	0.17	0.23	0.17	0.11	0.18	0.15
MgO	7.61	8.08	7.45	5.34	4.02	6.23	3.72	4.40	2.21	1.97	0.74
CaO	9.07	9.22	9.04	10.54	10.59	10.15	8.54	8.75	6.68	4.65	2.66
Na_2O	2.88	2.65	2.69	2.83	2.56	2.45	3.60	2.63	3.63	4.57	3.87
K_2O	0.94	0.82	0.92	0.61	0.36	0.53	0.58	1.12	2.16	1.53	3.14
P_2O_5	0.15	0.17	0.18	0.21	0.10	0.18	0.24	0.14	0.18	0.34	0.12
Ba	280	230	na	200	na	na	330	na	na	500	na
Co	35	39	na	28	na	na	38	na	na	14	na
S	73	70	na	80	na	na	120	na	na	120	na
V	190	220	150	180	180	200	250	200	170	120	72
Cr	460	700	600	57	41	82	bdl	70	26	bdl	bdl
Ni	120	140	100	42	11	45	24	28	18	21	20
Cu	59	110	80	66	24	110	110	79	100	52	43
Zn	73	84	65	65	66	80	96	80	72	120	68
Ga	12	13	14	12	11	12	17	12	14	20	13
Ge	2.4	3.0	1.3	1.9	2.2	1.8	3.5	2.3	1.7	2.1	2.1
Br	0.33	bdl	bdl	bdl	bdl	0.21	bdl	0.16	0.30	bdl	1.1
Rb	13	14	15	10	5.0	7.3	9.2	19	36	22	54
Sr	350	370	340	410	350	350	390	310	340	330	180
Y	22	22	22	18	18	22	27	23	32	46	40
Zr	91	93	91	72	50	68	79	100	180	170	160
Nb	1.7	2.1	2.2	1.4	0.8	1.5	1.3	1.7	3.3	3.7	4.6
Mo	0.74	0.70	0.94	0.41	0.37	0.47	0.51	0.92	1.50	0.86	2.1
Pd	bdl	bdl	bdl	0.12	bdl	bdl	0.09	bdl	bdl	bdl	bdl
Ag	0.34	0.52	0.46	0.51	0.20	0.35	0.57	0.30	0.25	0.30	0.25
Cd	0.29	0.43	12	0.40	0.17	0.40	0.46	0.28	bdl	0.58	0.25
Sn	2.1	1.1	1.3	1.1	1.0	1.2	1.4	2.4	5.9	2.3	2.8
Sb	0.31	0.42	0.40	0.25	0.42	0.38	0.47	0.56	1.10	0.39	1.40
Te	bdl	0.25	bdl	bdl	0.15	bdl	0.19	bdl	bdl	0.30	0.19
I	bdl	0.18	bdl	bdl	bdl	bdl	bdl	0.22	1.1	0.57	0.60
Cs	0.60	0.60	1.10	0.40	0.49	0.78	0.59	1.70	1.90	0.52	2.40
As	bdl	bdl	bdl	bdl	bdl	bdl	bdl	0.60	6.7	bdl	18
Pb	11	6.1	5.5	4.6	8.0	10	5.3	11	11	13	15
Th	2.9	2.4	3.9	2.5	2.6	2.2	2.8	2.4	4.5	3.1	4.8
U	0.90	bdl	1.1	bdl	bdl	0.78	bdl	bdl	2.1	1.7	3.6

Mg-bearing mineral precipitates at these low pH values at any of the observed or calculated temperatures (Varekamp et al., 2009).

Typically, high values of the enrichment factor indicate high mobility of elements in water–rock interactions. For the present case, the majority of elements have an enrichment factor $F_i \gg 1$, implying the intrusion of magmatic gases into pool solutions (Fig. 6). The elements Mn, Mg, Y, Ti, Zr, and Cu, with enrichment factors of approximately 0, can be released into solutions from host rocks during congruent rock dissolution by the action of magmatic gases. Only two elements, Si and Nb, which have log $F_i < 0$, are less mobile. Application of Fi in the analysis of element behavior in water–rock interaction is justified assuming steady-state conditions in the fluid during ascent through the host rocks. Nevertheless, the occurrence of geochemical barriers to the fluid routes can significantly complicate element partitioning between the fluid and the rocks; this complication completely changes the geochemistry of the water–rock interaction.

For example, at the subsurface barrier "pore solution–pool solution," trace element partitioning can be traced as a result of the phase separation of fluid into liquid and gas. In the remaining pore fluids, the concentrations of Fe, Al and Sb increase compared to those in the pool liquid by three orders of magnitude, those of As, Bi, Na, Mn, Co and Zr increase by more than two orders, and those of Sr, Cu, Ni, S, and Li increase by an order of magnitude (Fig. 7). A very similar process can be observed in the system "pore fluids of sulfur fumaroles–condensate," wherein almost all elements concentrate in the pore solutions relative to the vapor-gaseous mixture (condensate). Even such mobile components as the anion-forming elements As and Sb are not carried into the vapor-gaseous mixture but are retained in the pore fluids. Consequently, it is phase separation in the liquid state (rather than water–rock interaction) that might be the key mechanism governing the concentrations of elements in final hydrothermal manifestations, including boiling pools, springs and fumaroles.

4.4. Geophysical investigations

According to these results, the specific resistivity of media at the sites ranges from 0.1 to 10 Ohm m (Fig. 8). This low resistivity is related to the saturation of the media with highly saline thermal waters, while a high resistivity is a characteristic of media that are washed by thawed waters from the snowfield. The results allow suggesting that the zonation of electric resistivity is mainly caused by the TDS of the pore fluids. The influence of clays on the formation of zones may be considerable, as has been shown by Komori et al. (2010). Samples from hot sites were tested with reference to the map of the geo-electrical parameters that was prepared in 2007. It was established that the electric resistivity, TDS, and concentrations of some trace elements are clearly correlated (Manstein et al., 2008). For this reason, the geo-electrical cross section is interpreted as simply a change in the TDS of pore solutions, eliminating the need for additional geochemical analysis. The spatial distribution of conducting zones indicates the existence of subsurface vertical channels that are heavily saturated with highly saline

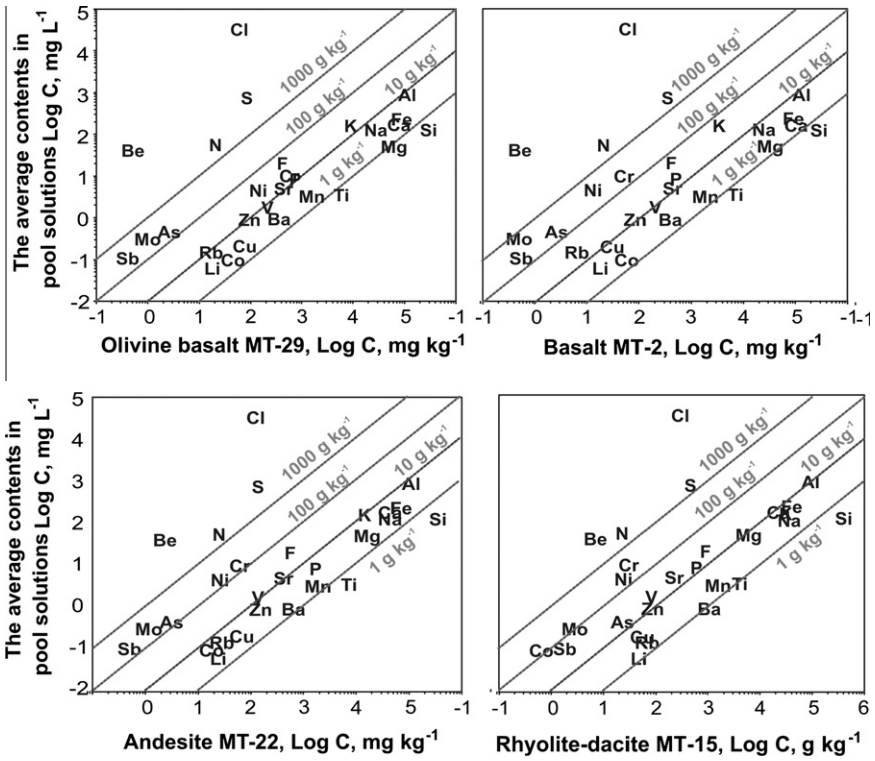

Fig. 5. Log-log plots for the concentrations of major and trace elements in pool liquids vs. those of different Mutnovsky lava flows. Elements that were detected in single samples (and are not tabulated) include Br, I, Bi, Te, Se, Ag, Cd, Y, Th, and Nb.

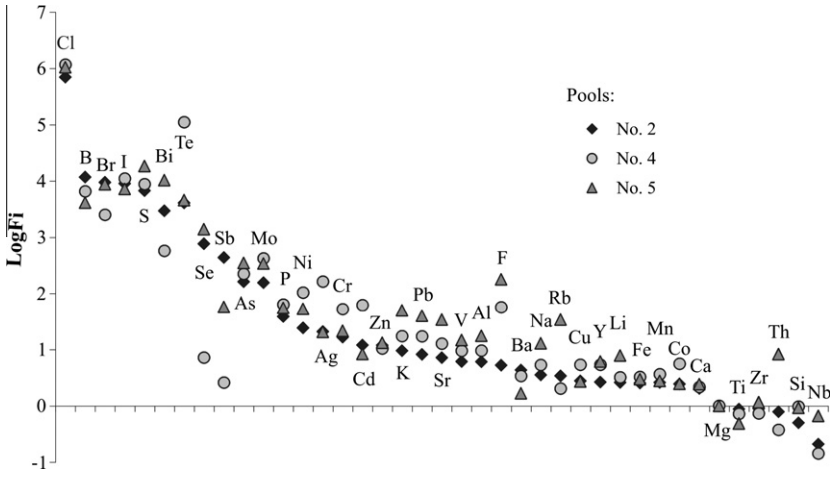

Fig. 6. Mg-normalized enrichment coefficients for major and trace elements.

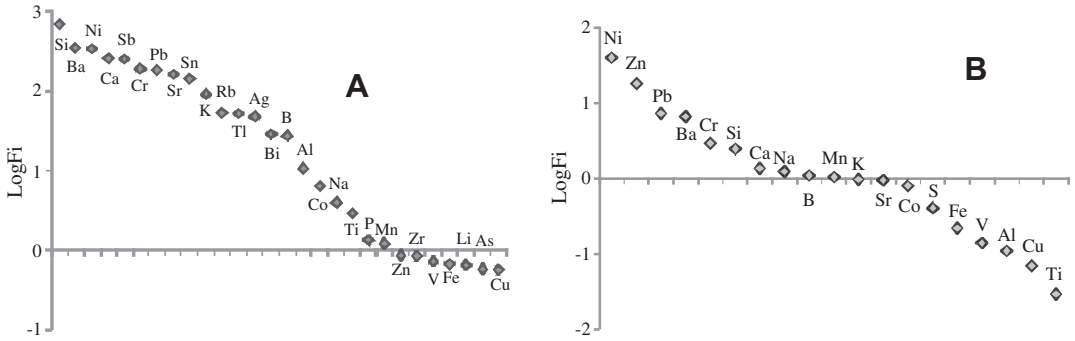

Fig. 7. Enrichment factors for elements in the following systems: "pore solutions of hot sites–liquids of mud pools" (A) and "pore solution of fumarole dome–condensate" (B).

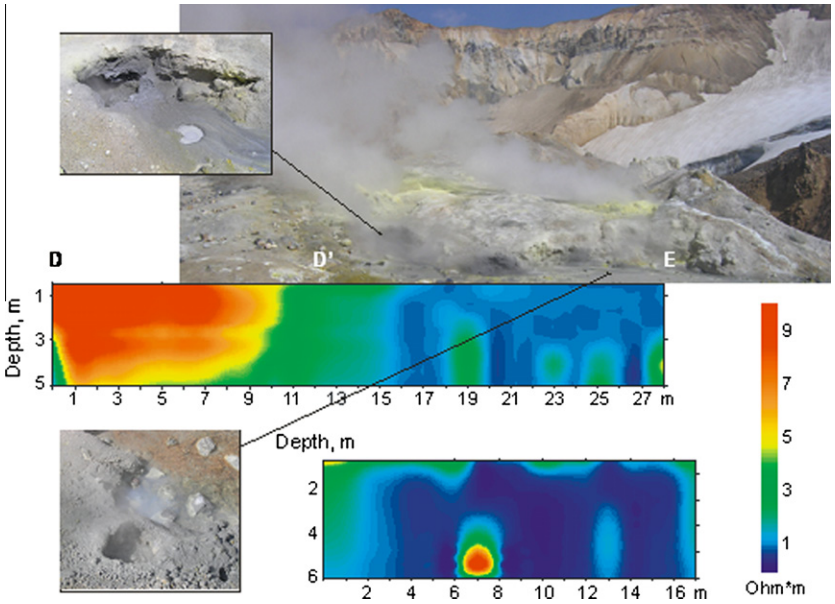

Fig. 8. Geo-electrical cross sections along the line of the mud pool position: the upper cross section was obtained in 2007, and the lower cross section was obtained in 2009.

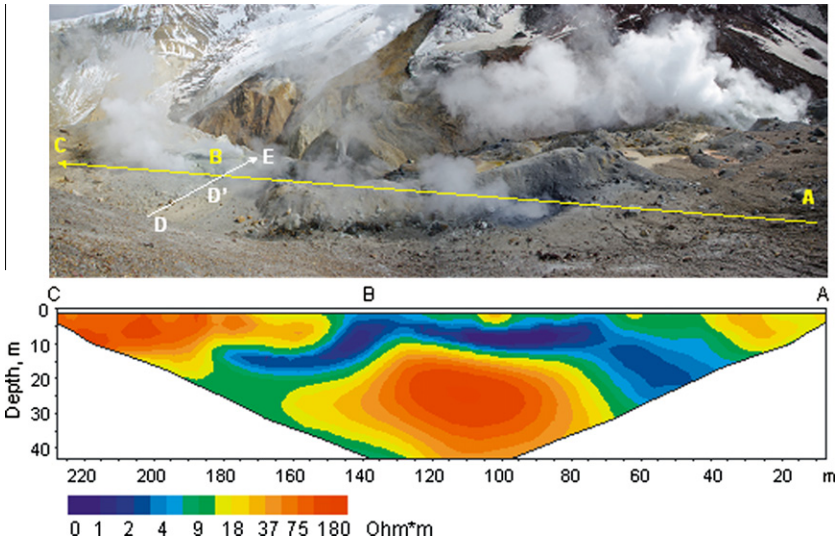

Fig. 9. Resistivity transect (AC) across the pool axis (DE).

thermal waters (blue colors in the cross sections). These zones correspond to mud pool-feeding channels. Vertical channels are separated from each other by walls of high electric resistivity that are 1–3-m thick. The walls can be formed of denser rocks that are less permeable to the fluid than are the bulk rocks. The resistivity profile shows that thermal waters reach the surface from a deep source beyond the range of the sounding technique. However, the structure of the feed channels (it is assumed that the sounding depth was approximately 6 m) denotes their stable vertical configuration. Media of high conductivity were interpreted as feed channels with highly saline brines, becoming narrower with increased distance from the source.

A comparison of the electromagnetic sounding results obtained in 2007 and 2009 shows two major findings. First, the vertical shape of the feed channels remains unchanged. Second, a hydrogeochemical zonation of the subsurface space has evolved: the zones of high conductivity became narrower, and the gradient of specific resistivity (ρ) for a similar area was higher in 2009 than in 2007.

In 2007, after a very snowy winter and a hot summer, when permanent snowfields were thawing intensively, large volumes

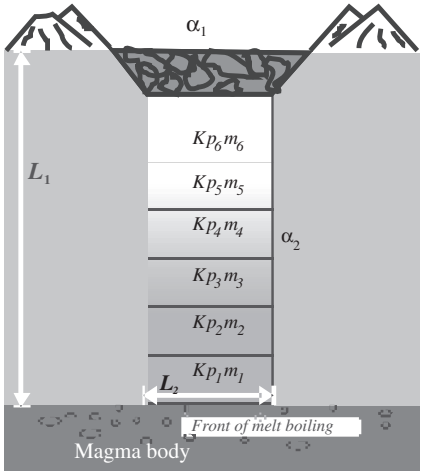

Fig. 10. Structural scheme of the model. *Kp* denotes permeability coefficient, m^2; *m* is porosity, %; α_1 and α_2 depict heat transfer coefficients at the upper boundary and the side surface of the fluid conductor, respectively; L_1 is the depth of the magma chamber; and L_2 is the width of the fluid conduit.

Table 5
Petrophysical characteristics of model layers.

Depth, m	A		B		C	
	Porosity, %	Permeability coefficient, m^2	Porosity, %	Permeability coefficient, m^2	Porosity, %	Permeability coefficient, m^2
100–0	10	10^{-13}	10	10^{-13}	10	10^{-13}
300–100	7.5	10^{-14}	7.5	10^{-14}	7.5	10^{-14}
500–300	5	10^{-15}	5	10^{-15}	5	10^{-15}
1500–500	3	10^{-15}	3	10^{-15}	3	10^{-15}
1800–1500	2	10^{-15}	1	10^{-16}	0.5	10^{-16}
2000–1800	1	10^{-15}	0.5	10^{-16}	0.1	10^{-17}

of fresh meteoric waters lowered the ratio of magmatic fluids to surface water, and these conditions changed the TDS and trace element concentrations. Thus, the mud pools were totally flooded, and the feed channels were "diffuse". In 2009, after a less snowy winter with no thawing snowfields, the ratio was higher than in 2007. These conditions caused the narrowing of feed channels and the appearance of relatively dry, more resistive "walls" between them. As a result, the TDS and trace element concentrations of the solutions increased. Another result of these events was a change in the hydrochemical subsurface zonation. In 2007, the subsurface media were commonly flooding volume. Such a situation can be evoked by the minimal influence of surface fresh (meteoric) waters. In this case, the composition of surface manifestation solutions will originate mainly in deep magmatic fluids coming to the surface.

Additional information for the understanding of pool origin can be obtained from the 2009 geo-electrical tomography data (Fig. 9). The resistivity tomography results show the conductive zones (resistivity from near zero to 20 Ohm m). They are located at depths of 6–25 m. According to the results all of the subsurface conductive zones are fed by brine from one reservoir. The presence of the boiling brine reservoir was suggested by Taran et al. (1991) based on the composition of a large black mud pool in the southern part of the Donnoe field. This hypothesis has been proven by the present investigation.

At particular parts of the observation profile (0–40 m, 95–105 m, and 155–230 m), the reservoir is overlapped by a non-permeable resistive layer. It can be suggested that the brines are formed due to the condensation of volcanic gases in deep horizons under a non-permeable layer at a depth of approximately 10–15 m. The less concentrated solutions are discharged at the surface through fractured zones (40–50 m, 65–90 m and 105–150 m). Thus, the results of a geo-electrical cross section can be interpreted as a manifestation of a shallow-depth phase barrier.

Therefore, the analysis of hydrothermal solution/host rock interactions indicates that even large-scale hydrothermal alteration cannot cause the large amounts of major and trace elements that are recorded in mud pool liquids at the Donnoe field. The inner structure of the feed channels accounts for a high geochemical contrast between the mud pools and provides evidence of deep roots of vertical channels for fluid ascent to the surface. To understand the origin of the mud pools and the nature of the high element concentrations, physicochemical modeling of the magmatic fluid/rock interactions on the way from the magma chamber to the surface expressions was performed.

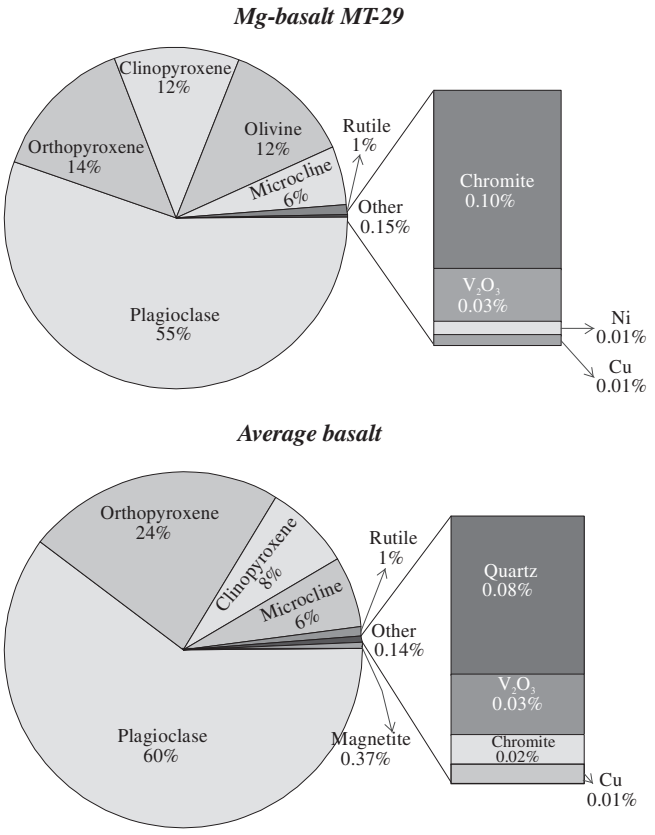

Fig. 11. Mineral composition of basalts under initial equilibrium (as a result of modeling).

Table 6
Chemical composition of the model.

	Average basalt	Mg-basalt
Bulk rock composition, ms (%)		
SiO_2	51.7	51.1
TiO_2	0.97	0.84
Al_2O_3	17.9	16.7
Fe_2O_3 total	9.77	9.73
MnO	0.17	0.15
MgO	4.43	7.61
CaO	8.54	9.07
Na_2O	3.15	2.88
K_2O	1.06	0.94
P_2O_5	0.22	0.15
Trace element (ppm)		
V	210	190
Cr	65.5	460
Ni	23.7	117
Cu	86.1	59
Zn	76.8	73
Ag	0.30	0.34
Sb	0.34	0.31
As	9.7	0
Pb	10.4	11
Gases, ms (%)		
H_2O	2.17	
Cl	0.168	
F	0.077	
S	0.134	

4.5. Physicochemical modeling

To understand the origin of the extremely high major, minor and trace element concentrations in the Mutnovsky mud pool solutions, a model was used that was initially designed by Karpov et al. (1997) and further developed by Sharapov et al. (2008) and Bessonova et al. (2010). This physicochemical model estimates the variations in petrophysical parameters and element behavior with respect to the structures of the volcano edifice. In the thermal system of the Mutnovsky volcano, there are several contrast zones of fractured discharges of magmatic fluids (Zelenski, 2003) and anomalous hydrothermal springs/mud pools (Bortnikova et al., 2007, 2009). The depth to a magma chamber, which can be a source of heat and fluids feeding fumaroles and springs, is expected to range from 1200 to 2000 m (Utkin et al., 2005). It should be noted that the activity of local thermal systems is generally altered by frequent explosive eruptions in this region (Selyangin, 1993). Each intense eruption may induce an unsteady stage in the geological structure. Consequently, the simulation of an unstable phase of a volcanogenic fluid–rock system life is mandatory for adequate modeling.

The scheme of the structural and mass balance model of the volcanic hydrothermal system is shown in Fig. 10. A high-permeability flat fractured zone (see individual rectangles on this diagram) bisects a stratified cross section of volcanic rocks and is characterized by variable porosity (m) and permeability (Kp).

The sides of the fluid conduction zone are impermeable in this model (zero mass transfer). Therefore, heat transfer between the fluid and the wall rocks is described through an effective heat transfer coefficient, α_2 (Sharapov et al., 2008). On the discharge surface, the heat transfer between magmatic fluid and the atmosphere is described by the heat emission coefficient, α_1. The initial temperature of the fluid is 1000 °C. The principal factors governing the temperature and pressure (T–P) dynamics in magmatic fluid systems are the location and number of impermeable layers (barriers) in fluid current zones. With these considerations, a series of different fluid transport zones structures were analyzed. In scenario A, only permeability increases towards the surface. In

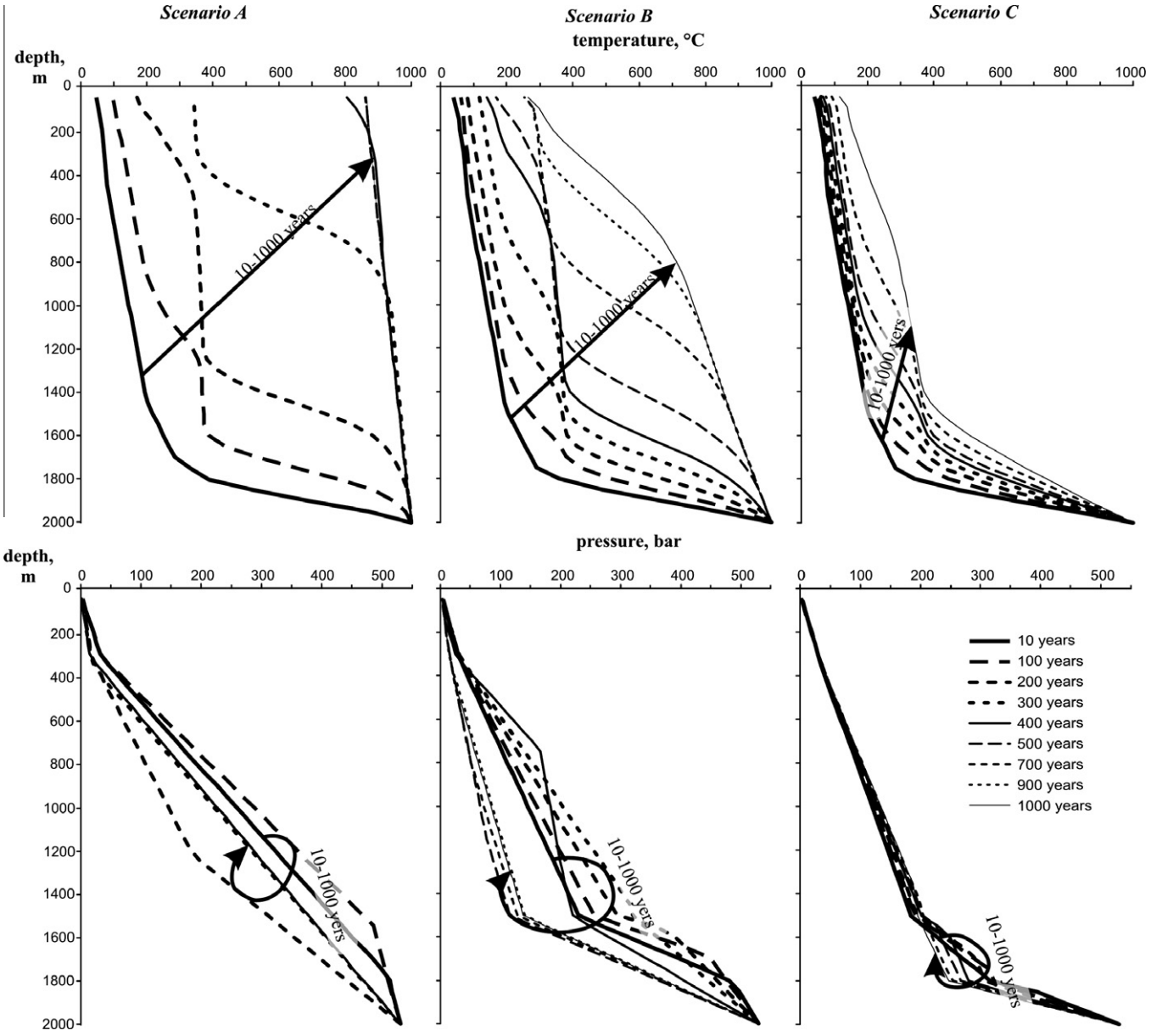

Fig. 12. Dynamics of temperatures and pressures in the cross section with respect to the fluid conduction structure.

scenario B, porosity and permeability increase gradually in an upward direction. In scenario C, a weakly permeable layer (solidifying crust) is on top of the magma chamber, but the porosity and permeability increase as in scenario B (Table 5).

The magmatic fluid ascending from the magma chamber moves through a chain of 40 reservoirs. Its composition corresponds to a mixture of volatile components recorded in glasses from basalt from the active continental edge. The chemical composition of reservoir 1 rocks corresponds to Mg-basalt MT-29. The composition of the overlying rocks is that of the average basalt of the Mutnovsky volcano (Table 4). The equilibrium mineral composition at the beginning of the rock–fluid interaction is shown in Fig. 11. The physicochemical dynamics of the fluid–rock interaction are described in a model of 40 uniformly distributed reactors in 50-m steps.

The model describes the physicochemical dynamics of the fluid–rock interaction by layering a chain of 40 uniform "reactors" buried at a depth of 2000 m with a step size of 50 m. The chemical composition of base reactor 1 is Mg-basalt MT-29. The composition of overlying rocks is the average basalt of the Mutnovsky volcano (Table 6). The composition of fluids corresponds to the mixture of volatile components recorded in melted inclusions and quenching glasses from the basalt of the active continental edge (Kovalenko et al., 2000). At the beginning of the rock–fluid interaction (initial conditions for the model), the equilibrium mineral composition is shown in Fig. 11.

The metals discussed above (Cr and Ni) are distributed in the following way. Chromium is present as chromites in both Mg-basalt and normal basalt. Nickel in Mg-basalt is native Ni (65%). The remaining Ni is admixed in olivine and orthopyroxene. In the

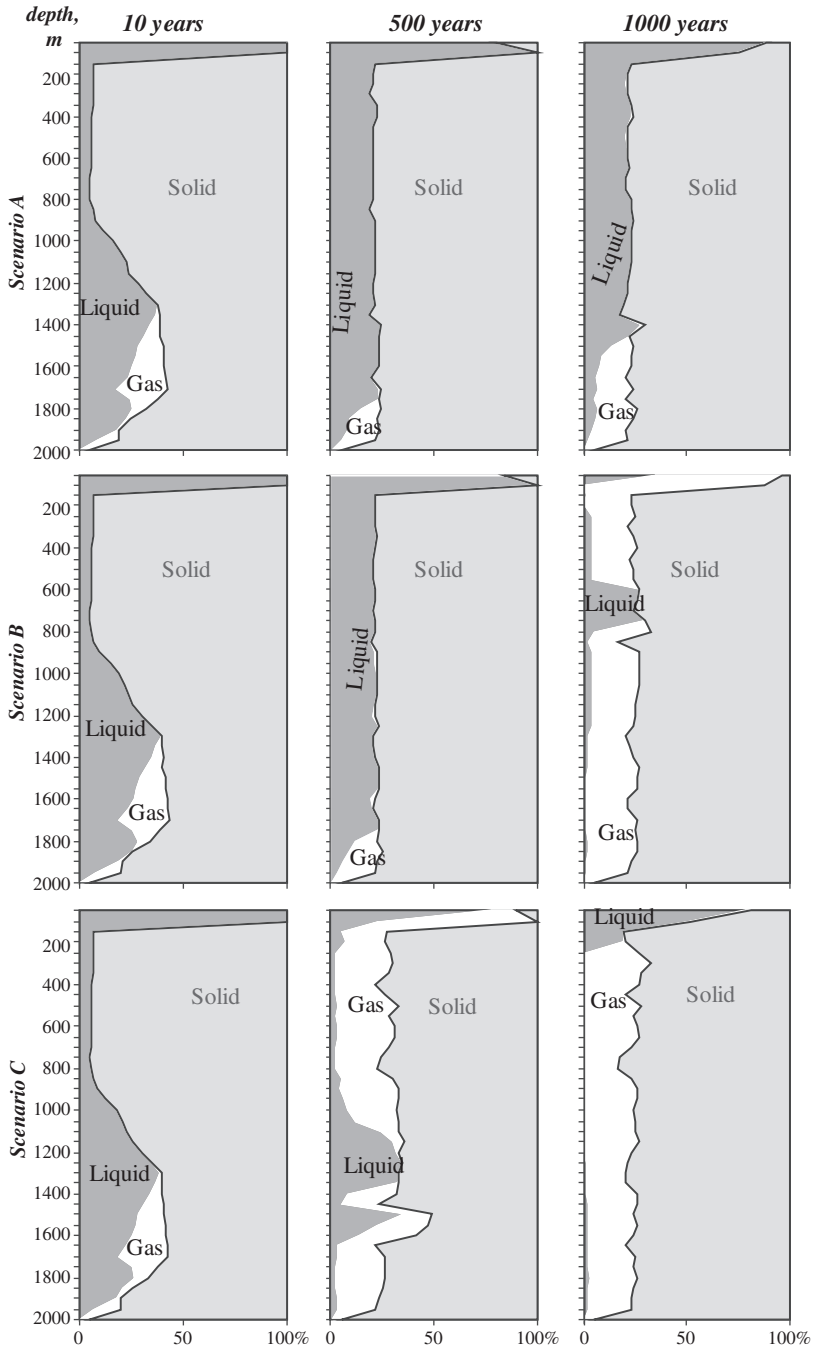

Fig. 13. Percentage of solution and gas in the fluid versus depth for different periods of hydrothermal system development.

overlying basalts, Ni occurs only in orthopyroxene. Vanadium in Mg-basalt forms V_2O_3, and Cu occurs as native Cu.

In scenario A, the temperature of the cross section varies irregularly. The heat from the magma chamber takes approximately 300 a to cause the extremely high temperatures on the surface, while in the deep cross section, the temperature is constant (Fig. 12). In scenario B, the heating of the cross section is more uniform. In the uppermost part, a moderate temperature controlling certain hydrothermal processes (260 °C) has become stable after 1 ka. Scenario C corresponds to a low-temperature hydrothermal process. Only at a depth of 1500 m do the temperatures reaches 300 °C, but in the uppermost part, the temperatures do not exceed 120 °C.

Phase separations in the fluid are a consequence of the temperature distribution (Fig. 13). The phase composition of a fluid is responsible for the main features of the processes taking place in the cross section. In scenario A, the prevalence of solutions over gas is possible only during the first 100 a of system development. Then, condensation of high saline brines will occur just beneath the surface. Scenario B is different with regard to phase separations. For the first 400 a of fluid life, the predominant phase is solution, but later, gases play an increasingly important role. The zone of fluid condensation commenced formation 700 a ago. The low-temperature scenario C is characterized by a complete prevalence of solutions from a depth of more than 1600 m.

At the Mutnovsky volcano, all three scenarios can be observed. In surface manifestations several hundred meters apart, low-, moderate-, and high-temperature systems can be traced. Comparison of modeling results, temperatures in fluid vents at the Mutnovsky crater (Zelenski, 2003; Taran et al., 1992), and sequences of explosive eruptions in the Active Funnel (Gavrilenko and Bortnikova, 2007) allow concluding that interference with the hydrodynamic conditions of the system takes place at depths of approximately 100–200 m. Therefore, it is expect that it will take less than 30–40 a to recover the temperature in fluid vents (with $T > 700$ °C). Temperature conditions in the Active Funnel are close to those of scenario A. Moderate-temperature thermal systems with multiple phase separations and a possibility of element accumulation correspond to the conditions in the mud pools at the Donnoe field (scenario B). Hydrotherms of fractured zone deposits feed productive wells at the Mutnovsky station, where there is an intrusive body at 3–4 km in depth, are all in agreement with scenario C.

The evolution of elements described by the multi-reactor model is discussed here. At the beginning of the hydrothermal processes (scenario B), very intense Cr leaching occurs by a magmatic fluid liquid phase. Accordingly, Cr remains in the solids in high-temperature zones during all processes. However, in moderate-temperature systems, Cr is soon to be leached from rocks in the lowest part of the cross section and re-deposited in hydrothermally altered rocks of the uppermost part over 100 a. Further portions of magmatic gases interact with enriched rocks, and secondary leaching takes metals into the hydrothermal process. Permeable fractured channels in the volcanic edifice are required to keep the concentration of magmatic gases constant during their ascent. The main Cr species in solution are CrO_2^- and CrO_4^{2-}. Extremely high Cr concentrations (up to 2 g/L) can be attained in surface solutions if: (i) rocks such as olivine basalts (with compositions MT-29 and MT-60) are present in the cross section, and (ii) there is no significant dilution of magmatic fluid by fresh waters. Such a high Cr concentration is impossible in real surface manifestations because only dilute solutions were investigated. The only source of metals in mud pools is a deep magmatic fluid, but the conditions during fluid ascent control the composition in surface manifestations.

Nickel is leached from rocks to a lesser extent than Cr, but it can migrate both with gases in the high-temperature part of the cross section and via solutions in the uppermost part. The maximum Ni concentrations are attained later than those of Cr (up to 300 a of system development) due to a significant heating of the cross section, i.e., the gas phase is predominant. If the main fluid phase is solution, then Ni attains its maximum concentration after 700 a. The major Ni species in solution are NiO and NiO_2^{2-}. In gases at high temperatures, the major Ni species are the halogenides NiF_2 and $NiCl_2$. In contrast to the patterns for Cr, Ni can form on the surface of its own mineral phases, such as native Ni and sulfides.

5. Conclusions

A comprehensive study (geochemical, geophysical and simulation) was carried out in the Donnoe fumarole field at the Mutnovsky volcano. The high TDS and trace element concentrations are controlled by the structural properties of the cross section through which the fluid ascends. The majority of trace elements whose concentrations in the pool solutions are high have been released from the magmatic gases concentrating on the phase barriers. The study reveals the presence of a shallow hydrothermal reservoir located at a depth of approximately 6–20 m and continuing by channels to depth of about 40 m. The variable surface discharges are fed from a common reservoir.

Annual variations can be explained by meteorological conditions. However, a high contrast in the concentrations between adjacent pools is caused by the complexity of the hydrogeochemical zonation of the subsurface space. A combination of geochemical and geophysical methods of investigation and physicochemical modeling make possible the development of a model for fluid–rock interactions and the origins of the surface manifestations.

Acknowledgements

The authors thank S. Nechepurenko, L. Trofimova, Yu. Kolmogorov, N. Karmanov for their analytical support in the Analytical Center of the Institute of Geology and Mineralogy of SB RAS and S. Kiyanov, N. Prisekina for kindly helping in the technical design of the manuscript. We acknowledge V. Sharapov, Yu. Taran, M. Zelenski, H. Ármannsson, and an anonymous reviewer for their contribution to constructive discussions of our study. This work was financially supported by grants from the President of Russian Federation (MK-167.2010.5), Russian Fund of Fundamental Researches (Grants N 09-05-00138) and the Siberian Branch of RAS (Grant No. 96).

References

Auippa, A., Allard, P., d'Alessandro, W., Michel, A., Parello, F., Treuil, M., Valenza, M., 2001a. Mobility and fluxes of major, minor and trace metals during basalt weathering and groundwater transport at Mt. Etna volcano (Sicily). Geochim. Cosmochim. Acta 64, 1827–1841.

Auippa, A., Dongara, G., Capasso, G., Allard, P., 2001b. Trace elements in the thermal groundwaters of Vulcano Island (Sicily). J. Volcanol. Geotherm. Res. 98, 189–207.

Baryshev, V.A., Kolmogorov, Y.P., Kulipanov, G.N., Scrinsky, A.N., 1986. X-ray fluorescent method with synchrotron radiation. J. Anal. Chem. 41, 389–401.

Bernard, A., Le Guern, F., 1992. Intrusive and basement rock sources of lead in hydrothermal systems of the Taupo Volcanic Zone, New Zealand. Geochim. Cosmochim. Acta 56, 2821–2829.

Bessonova, E.P., Sharapov, V.N., Chudnenko, K.V., Cherepanova, V.K., 2010. A new model of thermal and physico-chemical dynamics for volcanogenic epithermal deposits (Asacha deposit, Kamchatka). Doklady Earth Sci. 431, 453–457.

Bortnikova, S.B., Bessonova, E.P., Zelenskii, M.E., 2005. Hydrogeochemistry of Thermal Springs at Ebeco Volcano (Kuril Islands). In: Proc. World Geothermal Congress 2005. Antalia, Turkey, 24–29 April, CD.

Bortnikova, S.B., Gavrilenko, G.M., Bessonova, E.P., Lapukhov, A.S., 2009. The hydrogeochemistry of thermal springs on Mutnovskii Volcano, Southern Kamchatka. Volcanol. Seismol. 3, 388–404.

Bortnikova, S., Sharapov, V., Bessonova, E., 2007. Hydrogeochemical composition of springs at the Donnoe fumarole field, Mutnovsky volcano (Southern Kamchatka) and problems of their relation with supercritical magmatic fluids. Doklady Earth Sci. 413A, 410–414.

Delmelle, P., Bernard, A., 1994. Geochemistry, mineralogy and chemical modelling of the acid crater Lake of Kawah Ijen volcano, Indonesia. Geochim. Cosmochim. Acta 58, 2445–2460.

Fazlullin, S.M., 1999. Geochemical system of the Yuriev River, Kuril Islands: addition and removal of chemical elements. Volcanol. Seismol. 21, 79–99.

Finizola, A., Ricci, T., Deiana, R., Barde Cabusson, S., Rossi, M., Praticelli, N., Giocoli, A., Romano, G., Delcher, E., Suski, B., Revil, A., Menny, P., Di Gangi, F., Letort, J., Peltier, A., Villasante-Marcos, V., Douillet, G., Avard, G., Lelli, M., 2010. Adventive hydrothermal circulation on Stromboli volcano (Aeolian Islands, Italy) revealed by geophysical and geochemical approaches: implications for general fluid flow models on volcanoes. J. Volcanol. Geotherm. Res. 196, 111–119.

Fournier, N., Moreau, M., Robertson, R., 2011. Disappearance of a crater lake: implications for potential explosivity at Soufrière volcano, St Vincent. Lesser Antilles. Bull Volcanol.. doi:10.1007/s00445-010-0422-3.

Gavrilenko, G.M., Bortnikova, S.B., 2007. Hydrogeochemical monitoring at the active crater of the Mutnovsky volcano, Kamchatka, before and after the 2000 eruption. In: Bullen, T.D., Wang, Y. (Eds.), Water Rock Interaction 12. Proc. 12th Internat. Symp. Water–Rock Interaction, WRI-12. Taylor and Francis Group, London, pp. 77–80.

Giggenbach, W.F., 1996. Chemical composition of volcanic gases. In: Scarpa, R., Tillinh, R.I. (Eds.), Monitoring and Mitigation of Volcanic Hazards. Springer, Berlin, pp. 221–256.

Hedenquist, J.W., 1995. The ascent of magmatic fluid: discharge versus mineralization. Mineralogical Association of Canada. Short Course 23, 263–289.

Hinsberg, V., Berlo, K., Sumarti, S., Bergen, M., Williams-Jones, A., 2010. Extreme alteration by hyperacidic brines at Kawah Ijen volcano, East Java, Indonesia: II Metasomatic imprint and element fluxes. J. Volcanol. Geotherm. Res. 196, 169–184.

Karpov, I.K., Chudnenko, K.V., Kulik, D.A., 1997. Modeling chemical mass transfer in geochemical processes: thermodynamic relations. Conditions of equilibrium, and numerical algorithms. Am. J. Sci. 297, 767–806.

Karpov, I.K., Chudnenko, K.V., Kulik, D.A., Bychinskii, V.A., 2002. The convex programming minimization of five thermodynamic potentials other than Gibbs energy in geochemical modeling. Am. J. Sci. 302, 281–311.

Komori, S., Kagiyama, T., Hoshizumi, H., Takakura, S., Mimura, M., 2010. Vertical mapping of hydrothermal fluids and alteration from bulk conductivity: simple interpretation on the USDP-1 site, Unzen Volcano, SW Japan. J. Volcanol. Geotherm. Res. 198, 339–347.

Korzhinsky, M.A., Botcharnikov, R.E., Tkachenko, S.I., Steinberg, G.S., 2002. Decade-long study of degassing at Kudriavy volcano, Iturup, Kurile Islands (1990–1999): gas temperature and composition variations, and occurrence of 1999 phreatic eruption. Earth Planets Space 54, 337–347.

Kovalenko, V.I., Naumov, V.B., Yarmoluk, V.V., Dorofeeva, V.A., 2000. Volatile components (H_2O, CO_2, Cl, F, S) in magmas of moderate and acid composition at different geodynamic situations on the base of investigations of melted inclusions and quenching glasses. Petrology 8, 586–619.

Manstein, A.K., Epov, M.I., Voevoda, V.V., Sukhorukova, K.V., 1983. RF Patent Certificate 2152058. Bull, Izobret, 9.

Manstein, Y.A., Balkov, E.V., Manstein, A.K., Chemyakina, M.A., 2006. Electromagnetic frequency sounding for archaeological tasks application practice. Geophysika 1, 43–50.

Manstein, Y.A., Bortnikova, S.B., Manstein, A.K., Gavrilenko, G.M., Vernikovskaya, I.V., Sez'ko, N.P., 2008. Structure peculiarities of convective channels from thermal sources in Mutnovskii volcano (South Kamchatka). Doklady Earth Sci. 423A, 1404–1409.

Pasternack, G.B., Varekamp, J.C., 1994. The geochemistry of the Keli Mutu crater lakes, Flores, Indonesia. Geochem. J. 28, 243–262.

Rowe, G.L., Brantley, S.L., Fernández, J.F., Borgia, A., 1995. The chemical and hydrologic structure of Poás Volcano, Costa Rica. J. Volcanol. Geotherm. Res. 64, 233–267.

Selyangin, O.B., 1993. New data on Mutnovsky volcano: structure, evolution, development. Volcanol. Seismol. 1, 17–35.

Serafimova, E.K., 1979. Mineralogy of Sublimates at Kamchatka Volcanoes. Nauka, Moscow.

Sharapov, V.N., Cherepanov, A.N., Cherepanova, V.K., Bessonova, E.P., 2008. Dynamics of phase fronts in ore-forming fluid systems of volcanic arcs. Russ. Geol. Geophys. 49, 827–835.

Shinohara, H., Giggenbach, W.F., Kazahaya, K., Hedenquist, J.W., 1993. Geochemistry of volcanic gases and hot springs of Satsuma Iwojima, Japan: following Matsuo. Geochem. J. 27, 271–285.

Shinohara, H., Ohba, T., Kazahaya, K., Takahashi, H., 2008. Origin of volcanic gases discharging from a cooling lava dome of Unzen volcano, Japan. J. Volcanol. Geotherm. Res. 175, 133–140.

Symonds, R.B., Rose, W.I., Reed, M.H., Lichte, F.E., Finnegan, D.L., 1987. Volatilization, transport and sublimation of metallic and non-metallic elements in high temperature gases at Merapi Volcano, Indonesia. Geochim. Cosmochim. Acta 51, 2083–2101.

Symonds, R.B., Rose, W.I., Bluth, G.J., Gerlach, T. M., 1994. Volcanic-gas studies: methods, results and applications. In: Carrol, M.R., Holloway, J.R. (Eds.), Volatiles in Magmas. Rev. Mineral., vol. 26, pp. 1–66.

Takano, B., Fazlullin, S.M., Delmelle, P., 2000. Analytical laboratory comparison of major and minor constituents in an active crater lake. J. Volcanol. Geotherm. Res. 97, 497–508.

Taran, Y.A., Bernard, A., Gavilanesc, J.-C., Africano, F., 2000. Native gold in mineral precipitates from high-temperature volcanic gases of Colima volcano, Mexico. Appl. Geochem. 15, 337–346.

Taran, Y.A., Gavilanes, J.C., Cortes, A., 2002. Chemical and isotopic composition of fumarolic gases and the SO_2 flux from volcán de Colima, between the 1994 and 1998 eruptions. J. Volcanol. Geotherm. Res. 117, 105–119.

Taran, Y.A., Hedenquist, J.W., Korzhinsky, M.A., Tkachenko, S.I., Shmulovich, K.I., 1995. Geochemistry of magmatic gases of Kudryavy volcano, Iturup, Kuril Islands. Geochim. Cosmochim. Acta 59, 1741–1761.

Taran, Y.A., Pilipenko, V.P., Rozhkov, A.M., Vakin, E.A., 1992. A geochemical model for fumaroles of the Mutnovsky volcano, Kamchatka, USSR. J. Volcanol. Geotherm. Res. 49, 269–283.

Taran, Y.A., Rouwet, D., Inguaggiato, S., Aiuppa, A., 2008. Major and trace element geochemistry of neutral and acidic thermal springs at El Chichón volcano, Mexico. Implications for monitoring of the volcanic activity. J. Volcanol. Geotherm. Res. 178, 224–236.

Taran, Y.A., Vakin, E.A., Pilipenko, V.P., Rozhkov, A.M., 1991. Geochemical study in crater of Mutnovsky volcano. Volcanol. Seismol. 5, 37–55.

Taran, Y.A., Znamenskiy, V.S., Yurova, L.M., 1996. Geochemical model of the hydrothermal system of Baransky volcano, Iturup, Kuril Islands. Volcanol. Seismol. 17, 471–496.

Trukhin, Y.P., Stepanov, I.I., Shuvalov, R.A., 1986. Mercury in Recent Hydrothermal Process. Nauka, Moscow.

Utkin, I.S., Fedotov, S.A., Delemen, I.F., Utkina, L.I., 2005. Dynamics of growing and development of flowing magma chamber of Mutnovsky–Gorely volcanoes, their thermal fields and heat accumulation. Volcanol. Seismol. 6, 11–29.

Vakin, E.A., Kirsanov, I.T., Pronin, A.A., 1966. Active funnel of the Mutnovsky Volcano. Bull. Volcanol. Stant. 40, 25–36.

Varekamp, J.C., Ouimette, A.P., Herman, S.W., Flynn, K.S., Bermudez, A., Delpino, D., 2009. Naturally acid waters from Copahue volcano, Argentina. Appl. Geochem. 24, 208–220.

Villemant, B., Mouatt, J., Michel, A., 2008. Andesitic magma degassing investigated through H2O vapour–melt partitioning of halogens at Soufrière Hills Volcano, Montserrat (Lesser Antilles). Earth Planet. Sci. Lett. 269, 212–229.

Zelenski, M.E., 2003. Element Transport and Mineral Formation in Zones of High Temperature Fumaroles on Mutnovsky Volcano (Kamchatka), Ph.D. Thesis. Novosibirsk.

Zelenski, M., Bortnikova, S., 2005. Sublimate speciation at Mutnovsky volcano, Kamchatka. Eur. J. Mineral. 17, 107–118.

Zelenski, M., Taran, Y., 2011. Geochemistry of volcanic and hydrothermal gases of Mutnovsky volcano, Kamchatka: evidence for mantle, slab and atmosphere contributions to fluids of a typical arc volcano. Bull. Volcanol.. doi:10.1007/s00445-011-0449-0.

Zelenski, M.E., Ovsyannikov, A.A., Gavrilenko, G.M., Senyukov, S.L., 2002. Eruption of the Mutnovsky volcano (Kamchatka) at March 2000. Vulcanol. Seismol. 6, 25–28.

Zlotnicki, J., Sasai, Y., Toutain, J.P., Villacorte, E., Harada, M., PHIVOLCS Team, Yvetot, P., Fauquet, F., Bernard, A., Nagao, T., 2009. Electromagnetic and geochemical methods applied to investigations of hydrothermal/volcanic unrests: examples of Taal (Philippines) and Miyake-jima (Japan) volcanoes. Phys. Chem. Earth 34, 394–408.